

# Unifying Interacting Nodal Semimetals: A New Route to Strong Coupling

Shouvik Sur<sup>1,2</sup> and Bitan Roy<sup>3</sup>

<sup>1</sup>*Department of Physics & Astronomy, Northwestern University, Evanston, IL 60208, USA*

<sup>2</sup>*National High Magnetic Field Laboratory and Department of Physics,  
Florida State University, Tallahassee, Florida 32306, USA*

<sup>3</sup>*Max-Planck-Institut für Physik komplexer Systeme, Nöthnitzer Str. 38, 01187 Dresden, Germany*  
(Dated: December 17, 2018)

We propose a general framework for constructing a large set of nodal-point semimetals by tuning the number of linearly ( $d_L$ ) and (at most) quadratically ( $d_Q$ ) dispersing directions. By virtue of such a unifying scheme, we identify a new perturbative route to access various strongly interacting non-Dirac semimetals with  $d_Q > 0$ . As a demonstrative example, we relate a two dimensional anisotropic semimetal with  $d_L = d_Q = 1$ , describing the topological transition between a Dirac semimetal and a normal insulator, and its three dimensional counterparts with  $d_L = 1$ ,  $d_Q = 2$ . We address the quantum critical phenomena and emergence of non-Fermi liquid states with unusual dynamical structures within the framework of an  $\epsilon$  expansion, where  $\epsilon = 2 - d_Q$ , when these systems reside at the brink of charge- or spin-density-wave orderings, or an  $s$ -wave pairing. Our results can be germane to two-dimensional uniaxially strained optical honeycomb lattice,  $\alpha$ -(BEDT-TTF)<sub>2</sub>I<sub>3</sub>.

*Introduction:* Over the last decade, semimetals with a discrete number of band touching or nodal points have become increasingly important for the understanding of topological phases of matter [1–4]. In this paradigm, Dirac semimetals (DSMs), realized as a stable phase of matter or at a critical point separating two topologically distinct insulators, play an important role [5]. Semimetals are, however, more general states of matter [6], and the bands in the neighborhood of the nodes may develop finite curvatures along one or more directions, see Fig. 1. A positive band-curvature enhances the low energy density of states (DoS), which in turn strengthens the effects of Coulomb interactions. Therefore, semimetallic systems, falling outside the realm of linearly dispersing Dirac fermions, constitute a rich ground for exotic emergent phenomena, which we unveil (mainly) for an interacting two-dimensional anisotropic semimetal (ASM), displaying both linear and quadratic band dispersions, see Fig. 2. Our results can be relevant for uniaxially strained optical honeycomb lattice [7–9],  $\alpha$ -(BEDT-TTF)<sub>2</sub>I<sub>3</sub> [10], black phosphorus [11] and at the TiO<sub>2</sub>/VO<sub>2</sub> interface [12, 13], subject to strong Hubbard-like interactions [14]. Throughout we neglect the long-range tail of the Coulomb interaction [15, 16], which is justified for ultracold fermionic atoms in optical lattices or in the presence of a screening/proximate gate.

Traditionally the spatial dimensionality is tuned to gain insights into the strongly coupled bosonic and fermionic phases of matter [17–19]. For example, strong interactions between fermionic and bosonic (such as a collective mode) degrees of freedom can be addressed in terms of the deviation from a three-dimensional DSM (3d-DSM) along the horizontal dotted line in Fig. 1. In a 3d-DSM the boson-fermion Yukawa interactions are dimensionless or *marginal* in the language of renormalization group (RG) [20]. Here we formulate a distinct approach that ties together a wide class of in-

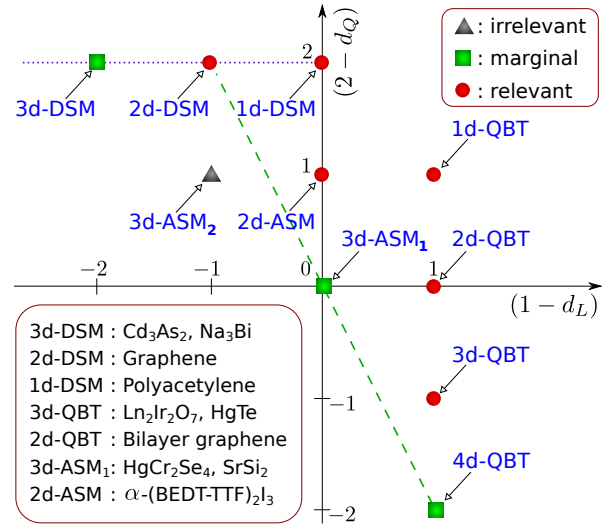


FIG. 1: Ten classes of nodal-point semimetals, distinguished by the number of linearly ( $d_L$ ) and quadratically ( $d_Q$ ) dispersing directions. Here DSM, ASM and QBT denote Dirac, anisotropic and quadratic band touching semimetals, respectively. The Yukawa coupling is marginal on the dashed line, separating the fixed points where it is relevant (filled circles) and irrelevant (filled triangle). Around this line the quantum fluctuations engendered by the Yukawa vertex are weak, and can be controlled by an  $\epsilon$  expansion. The  $d_Q = 0$  line is special due to the presence of full spacetime Lorentz symmetry. Lower inset: Material realizations of various semimetals.

teracting nodal semimetals by continuously varying the number of quadratically ( $d_Q$ ) and linearly ( $d_L$ ) dispersing directions, as shown in Fig. 1. This classification scheme allows us to identify (1) a three-dimensional ASM with  $d_L = 1$  and  $d_Q = 2$  (3d-ASM<sub>1</sub>) and (2) a four-dimensional quadratic band touching or Luttinger semimetal (4d-QBT) with  $d_L = 0$  and  $d_Q = 4$ , as two fixed points residing on a ‘marginal line’ (dashed line in

Fig. 1), along which the Yukawa coupling is dimensionless. Around the ‘marginal line’ the quantum fluctuations are under perturbative control, allowing us to access the effects of strong electronic interactions by suitable  $\epsilon$  expansions, where  $\epsilon$  measures the deviation from this line. As a demonstrative example, we here address the quantum criticality for a strongly interacting two-dimensional ASM (with  $d_L = d_Q = 1$ ) by performing an  $\epsilon$  expansion about 3d-ASM<sub>1</sub>, with  $\epsilon = 2 - d_Q$ . Our results are summarized in Table I and a schematic phase diagram is shown in Fig. 2. A full spatial rotational symmetry is present only along the  $d_L = 0$  line (besides the  $d_Q = 0$  line along which a Lorentz symmetry is present), which we will explore in future following the general theoretical framework developed in this work [21].

*Model:* The effective single particle Hamiltonian describing a  $d$ -dimensional generic nodal-point semimetal in a noninteracting system is given by

$$H_0(k_i) = \sum_{l=1}^{d_L} \Gamma_l k_l + \sum_{n=1}^{n_{\max}} \Gamma_{d_L+n} \varepsilon_n(k_{d_L+1}, \dots, k_d), \quad (1)$$

where  $k_i$  are components of momentum (measured from the band touching point),  $\{\Gamma_i\}$  is a set of mutually anti-commuting matrices,  $\varepsilon_n$  are quadratic functions of their arguments,  $d = d_L + d_Q$  and  $n_{\max} \leq d_Q$ . Short-ranged or Hubbardlike interactions can trigger a symmetry breaking phase by generating a mass term  $\sum_a M_a \Upsilon_a$ , where  $\{\Upsilon_a\}$  is another set of mutually anticommute matrices, satisfying  $\{\Upsilon_a, \Gamma_i\} = 0$ . Onset of such an ordering leads to a fully gapped state and the magnitude of  $\vec{M}$  determines condensation energy gain. Here we focus on the quantum critical point (QCP) controlling such a transition.

The effective action in the vicinity of the QCP at intermediate energies takes the form

$$\begin{aligned} \tilde{S} = & \sum_{n=1}^{N_f} \int_k \psi_{n,k}^\dagger G_0^{-1}(k) \psi_{n,k} + \int_q \frac{\text{Tr}(\vec{\phi}_{-q} \cdot \vec{\Upsilon})(\vec{\phi}_q \cdot \vec{\Upsilon})}{2 \text{Tr}\{\Upsilon_a^2\} \tilde{D}_0(q)} \\ & + \frac{g_0}{\sqrt{N_f}} \sum_{n=1}^{N_f} \int_{k,q} \vec{\phi}_q \cdot (\psi_{n,k+q}^\dagger \vec{\Upsilon} \psi_{n,k}) + \dots \quad (2) \end{aligned}$$

where  $k \equiv (k_0, k_1, \dots, k_d)$ , with  $k_0$  being the Euclidean frequency. Here,  $\psi_{n,k}$  ( $\vec{\phi}_q$ ) is a Grassman (real vector) field that represents the  $n^{\text{th}}$  copy of the fermionic modes (order parameter),  $g_0$  accounts for the Yukawa interaction, and the ellipses represent higher order terms (including  $u|\vec{\phi}|^4$ ) that are unimportant for the present analysis. We introduce  $N_f$  copies of fermions. The bare fermionic and bosonic propagators are  $G_0(k) = [ik_0 + H_0(k_1, \dots, k_d)]^{-1}$  and

$$\tilde{D}_0(q) = \left[ c^2 \left( q_0^2 + \sum_{l=1}^{d_L} q_l^2 \right) + \sum_{n=d_L+1}^{d_Q} q_n^2 + |\vec{M}|^2 \right]^{-1},$$

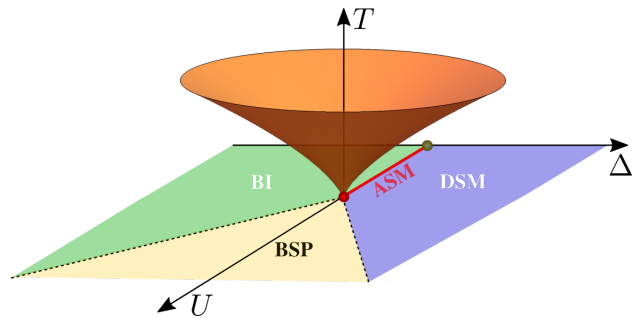


FIG. 2: A schematic finite temperature ( $T$ ) phase diagram of a two dimensional interacting ASM (realized along the red line), separating a DSM and a band insulator (BI). In a noninteracting system ( $U = 0$ ) the transition between these two phases takes place through a quantum critical point (QCP) located at  $\Delta = 0$  (gray circle). For sufficiently strong interaction ( $U$ ) a broken symmetry phase (BSP) sets in through a multicritical point (red circle), where DSM, BI, ASM and a BSP meet. Universality classes of various transitions (ASM-BSP and DSM-BI) across this fixed point are summarized in Table I. The critical cone accommodates a quasiparticleless metallic state (non-Fermi liquid).

respectively. The parameter  $c$  encodes an anisotropy of the bosonic dynamics, stemming from the anisotropic fermionic dispersing (when  $d_Q > 0$ ). Therefore, it is convenient to define a  $(d_L + 1)$ -dimensional frequency-momentum vector  $\mathbf{k} \equiv (k_0, k_1, \dots, k_{d_L})$  and a  $d_Q$ -dimensional momentum  $\mathbf{K} \equiv (k_{d_L+1}, \dots, k_d)$ .

The non-interacting part of the action is invariant under the scaling  $[\mathbf{K}] = 1$  and  $[\mathbf{k}] = z_{\mathbf{k}}$ , leading to

$$[c] = 1 - z_{\mathbf{k}}, [M] = 1, [g_0] = 1 - \frac{z_{\mathbf{k}}(d_L - 1) + d_Q}{2}. \quad (3)$$

The non-interacting fixed point possesses a full spacetime Lorentz symmetry only when  $d_Q = 0$  and  $z_{\mathbf{k}} = 1$ , implying that the Yukawa coupling is marginal for  $d_L = 3$ , which represents a three-dimensional DSM. For  $d_Q > 0$ , the Lorentz invariance is lost, and the fermionic DoS dominates over the bosonic one, which is further amplified in the large- $N_f$  limit. Hence, we set  $z_{\mathbf{k}} = 2$  at the non-interacting fixed point such that the fermionic propagator remains invariant under the tree-level scaling. For  $d_Q > 0$ , the Yukawa coupling is marginal on the line,  $2d_L + d_Q = 4$ , which passes through  $(d_L, d_Q) = (1, 2)$  and  $(0, 4)$ , respectively representing a 3d-ASM<sub>1</sub> and a 4d-QBT (see Fig. 1). Also note that for  $d_Q > 0$ ,  $[u] = 4 - \{2(d_L + 1) + d_Q\}$  which makes the  $|\vec{\phi}|^4$  terms irrelevant for non-Dirac semimetals.

*$\epsilon$  expansion:* We now focus on the QCP, residing on the critical hyperplane  $|\vec{M}|^2 = 0$ . Since the  $d_Q = 0$  line, representing DSMs, is relatively well understood [20], we focus on the  $d_Q > 0$  region, see Fig. 1. The deviations from the ‘marginal line’ [defined by  $[g_0] = 0$ , see Eq. (3)] along  $d_L$  and  $d_Q$  can be, respectively, parameterized by

	$N_b = 1$	$N_b = 2$	$N_b = 3$
$g_*^2/(2\pi^2)$	$f_1(N_f) \epsilon^{1+1/N_f}$	$(1 - \frac{1}{N_f}) \epsilon$	$f_3(N_f) \epsilon^{1-1/N_f}$
$z_{\mathbf{k}}$	$2 + \frac{1}{2N_f} \epsilon \ln \epsilon$	$2 + \frac{1}{N_f} \epsilon \ln \epsilon$	$2 + \frac{3}{2N_f} \epsilon \ln \epsilon$
$\eta_\psi$	$-\frac{3}{4N_f} \epsilon \ln \epsilon$	$-\frac{1}{2N_f} \epsilon \ln \epsilon$	$-\frac{9}{4N_f} \epsilon \ln \epsilon$
$\eta_\phi$	$-\frac{1}{2N_f} \epsilon \ln \epsilon$	$-\frac{1}{N_f} \epsilon \ln \epsilon$	$-\frac{3}{2N_f} \epsilon \ln \epsilon$
$\nu_M^{-1} - 2$	$-\epsilon$	$-\epsilon$	$-\epsilon$
$\nu_\Delta^{-1} - 2$	$\frac{1}{N_f} \epsilon \ln \epsilon$	$\frac{2}{N_f} \epsilon \ln \epsilon$	$\frac{3}{N_f} \epsilon \ln \epsilon$

TABLE I: Fixed points (first row), anomalous dimensions ( $z_{\mathbf{k}}, \eta_\psi, \eta_\phi$ ) and correlation length exponents ( $\nu_M, \nu_\Delta$ ), obtained in the limit  $\epsilon \ll 1, N_f \gg 1$ , where  $\epsilon = 2 - d_Q$  and  $N_f$  counts fermion flavor number [22, 23]. Respectively  $N_b = 1, 2$  and 3 are pertinent near charge-density-wave, superconducting  $s$ -wave and spin-density-wave orderings. Note  $\nu_M$  and  $\nu_\Delta$  are the correlation length exponents for ASM-BSP and DSM-BI quantum phase transitions, respectively, see Fig. 2.

$\epsilon_L = \bar{d}_L - d_L$  and  $\epsilon_Q = \bar{d}_Q - d_Q$ , where  $2\bar{d}_L + \bar{d}_Q = 4$ , and  $\epsilon_L$  and  $\epsilon_Q$  can be tuned independently to reach various interacting fixed points where the Yukawa coupling ( $g_0$ ) is dimensionful. At the formal level, it is accomplished through the dimensional regularization, and the RG equations can be derived within the minimal subtraction scheme. Due to the absence of the Lorentz invariance, our methodology differs substantially from the ones applied to DSMs. Owing to its novelty, we first highlight the key features of the formalism.

The tree-level scale invariance of the fermion propagator comes at the cost of  $c$  being strongly irrelevant [see Eq. (3)]. Thus,  $c^{-1}$  acts like a momentum scale, regulating divergences in diagrams involving the bare boson propagator. In the regime, where a perturbative expansion is controlled, the quantum corrections are generally weak and they cannot compensate a strong negative tree-level scaling dimension. Therefore within the perturbative window  $c$  flows to zero. Anticipating this fate, we set  $c = 0$  from outset [24]. The bosonic propagator then simplifies to  $D_0^{-1}(q) = |\mathbf{Q}|^2$ . In order to obtain a well-defined infrared (IR) scaling limit, physical quantities cannot be singular in  $c$  and the spurious divergences arising at  $c = 0$  are eliminated once IR adjustments are taken into account. To this end we implicitly resum an entire series of diagrams, shown in Fig. 3 [25]. This procedure is equivalent to replacing each bare boson propagator within a given Feynman diagram by a suitably dressed ultraviolet finite counterpart, and depending on the low energy DoS, it either Landau damps or screens the boson dynamics.

*Interacting ASM:* To exemplify the framework discussed so far, we focus on 3d-ASM<sub>1</sub>, with  $d_L = 1$  and  $d_Q = 2$ . Two physically relevant systems describing such an ASM are (1) the topological QCP separating a nodal-line semimetal and a BI [26–28], and (2) double Weyl semimetal [29, 30]. We focus on the former system, for

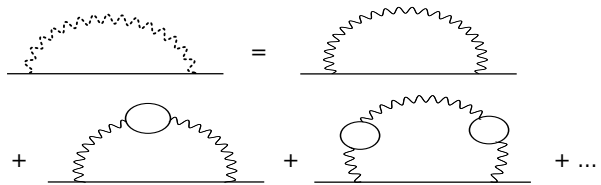


FIG. 3: Implicit resummation of diagrams in the RG analysis that cuts off infrared divergences arising in the  $c \rightarrow 0$  limit. The dotted (solid) wiggly and solid lines represent the dressed (bare) boson and fermion propagator, respectively.

which the effective single-particle Hamiltonian reads

$$H_0(k_x, k_y, k_z) = \sigma_0 [k_x \tau_1 + (k_y^2 + k_z^2 - \Delta) \tau_2]. \quad (4)$$

Two sets of Pauli matrices  $\{\sigma_\mu\}$  and  $\{\tau_\mu\}$  respectively operate on the spin and sublattice/orbital degrees of freedom, where  $\mu = 0, \dots, 3$ . Respectively for  $\Delta > 0$  and  $\Delta < 0$  the system describes a nodal-loop semimetal of radius  $\sqrt{|\Delta|}$  and a band insulator (BI). The transition between these two phases takes place at  $\Delta = 0$  and described by 3d-ASM<sub>1</sub>. In the absence of  $k_z$ , the above single-particle Hamiltonian captures the transition between a two-dimensional DSM and a BI [31]. Therefore, emergent quantum critical phenomena in a strongly interacting 2d-ASM with  $d_L = d_Q = 1$  can be addressed by performing a suitable  $\epsilon$  expansion about its three dimensional counterpart, more about which in a moment. At the topological QCP,  $\Delta$  is a relevant perturbation and plays the role of a tuning parameter.

For sufficiently strong interactions, the ASMs can terminate at a multicritical point, where a gapless topological phase (DSM or nodal-loop semimetal), BI, ASM and a broken symmetry phase meet, see Fig. 2. If we set the renormalized value of  $\Delta$  to be zero, the effective action at an intermediate momentum scale  $\mu$  takes the form

$$S = \sum_{n=1}^{N_f} \int_k \psi_{n,k}^\dagger G_0^{-1}(k) \psi_{n,k} + \frac{1}{2} \int_q |\mathbf{Q}|^2 (\vec{\phi}_{-q} \cdot \vec{\phi}_q) + \frac{g\mu^{(2-d_Q)/2}}{\sqrt{N_f}} \sum_{n=1}^{N_f} \sum_{j=1}^{N_b} \int_{k,q} \phi_q^j (\psi_{n,k+q}^\dagger \Upsilon_j \psi_{n,k}), \quad (5)$$

where  $g \equiv g_0 \mu^{(d_Q-2)/2}$  is the dimensionless Yukawa coupling. In the close proximity to the charge- and spin-density wave ordering  $N_b = 1$  and 3, and  $\Upsilon = \sigma_0 \tau_3$  and  $\sigma \tau_3$ , respectively. With an appropriate redefinition of the spinor basis the above effective theory is applicable near an  $s$ -wave pairing, for which  $N_b = 2$  and  $\Upsilon = \sigma_\perp \tau_3$ , where  $\sigma_\perp = (\sigma_1, \sigma_2)$ . Within the framework of an extended Hubbard model, containing onsite (repulsive and attractive) and nearest-neighbor interactions, these three phases are the most prominent ones [14, 27, 32, 33].

The Yukawa coupling becomes progressively more relevant as  $d_Q \rightarrow 1$ , the effects of which are systematically

incorporated by an  $\epsilon$  expansion, where  $\epsilon \equiv \epsilon_Q = 2 - d_Q$ . The ‘small’ parameter  $\epsilon$  measures the deviation from the upper critical dimension  $d_Q = 2$ , where  $[g_0] = 0$  for  $d_L = 1$ . In the neighborhood of the upper critical dimension the non-analyticities resulting from the anisotropic dispersion decouple from those originating from the relevance of  $g$  at the leading order, and allows a more controlled access to the asymptotically low energy physics. In addition, tuning  $d_Q$  in Eq. (5) offers two important advantages: (i) the number of Pauli matrices necessary for defining the  $d$ -dimensional local critical theory is independent of  $d$ , which allows  $d$  to be truly arbitrary, and (ii) the interaction vertex does not break the rotational symmetry in the  $\mathbf{k}$  or  $\mathbf{K}$  subspace, implying that the dynamical critical exponent defined with respect to the linearly dispersing direction is fixed at *unity*.

*RG & Fixed points:* Here the dominant IR processes that cut off the putative divergences in the  $c \rightarrow 0$  limit occur in the RPA channel, and implicit resummation [see Fig. 3] discussed above amounts to replacing  $D_0^{-1}(q)$  by the damped bosonic propagator  $D^{-1}(q) = |\mathbf{Q}|^2 + g^2|\mathbf{q}|/16$  [34]. Even though the resultant dynamics lacks point-like bosonic excitations, the fermions are still weakly coupled to the bosons, and to the linear order in  $\epsilon$ , we obtain the following RG flow equation for  $g$

$$\frac{dg}{d \ln \mu} = \frac{\epsilon}{2} g - \frac{g^3}{4\pi^2} \left[ 1 + \frac{3N_b - 4}{2N_f} + \frac{N_b - 2}{N_f} \ln \left( \frac{g^2}{16} \right) \right]. \quad (6)$$

While the vertex correction vanishes for  $N_b = 2$ , it screens (anti-screens) the Yukawa vertex for  $N_b = 1(3)$  [35]. The unusual  $\ln g^2$  terms results from the dynamical IR adjustments, and reflects that a naive perturbative expansion around the non-interacting fixed point cannot access the asymptotically low energy regime [34].

The non-interacting fixed point at  $g^2 = 0$  is stable for  $\epsilon = 0$  and  $N_b = 1, 2$ . But, a stable interacting fixed point is found at  $g_*^2 = 16e^{-(N_f+5/2)}$  when  $N_b = 3$ . This interacting fixed point is stabilized by a balance between the anomalous dimensions and vertex correction, and is inaccessible within a naive one-loop expansion. Therefore, in a three-dimensional interacting nodal-loop semimetal, residing in the close proximity to a topological QCP, only the transition to a spin-density-wave phase can be non-Gaussian in nature. By contrast, for  $d_Q < 2$  stable IR fixed points are obtained for  $N_b = 1, 2$  and 3. In order to simplify the results, we take the large  $N_f$  limit at fixed  $\epsilon$  and retain the leading order terms in  $1/N_f$ . The results are displayed in Table I. The stable fixed point at the superconducting or XY QCP is conventional as  $g_*^2 \propto \epsilon$ , whereas the quantum fluctuations are weakened (strengthened) in the neighborhood of the interacting fixed point for the charge(spin)-density-wave QCP.

*Non-Fermi liquid:* The leading order RG analysis also

yields the following nontrivial anomalous dimensions

$$z_{\mathbf{k}} = 2 + a\bar{g}^2, \quad \eta_\psi = -b\bar{g}^2, \quad \eta_\phi = - \left( a - 2\frac{N_f}{N_b} \right) \bar{g}^2, \quad (7)$$

where  $\bar{g}^2 \equiv \frac{N_b}{2N_f} \frac{g^2}{(2\pi)^2}$ ,  $a = 7 + 2 \ln(g^2/16)$  and  $b = 10 + 3 \ln(g^2/16)$  [34]. While  $z_{\mathbf{k}}$  controls the curvature of the dispersion according to  $E_\pm(k_x, \mathbf{K}) \sim \pm \sqrt{k_x^2 + |\mathbf{K}|^{2z_{\mathbf{k}}}}$ , the fermionic ( $\eta_\psi$ ) and bosonic ( $\eta_\phi$ ) anomalous dimensions, respectively, modify the corresponding two-point correlation function according to  $\langle \psi_{\mathbf{k}} \psi_{\mathbf{k}}^\dagger \rangle \propto |\mathbf{k}|^{-1+2\eta_\psi}$  and  $\langle \phi_{\mathbf{k}} \phi_{-\mathbf{k}} \rangle \propto |\mathbf{k}|^{-1+2\eta_\phi}$ . Hence, the residue of the quasiparticle (fermionic and bosonic) pole vanishes at this fixed point, indicating emergence of a non-Fermi liquid in its close vicinity. Since the anomalous dimensions of the fields are positive (see Table I), compared to the non-interacting limit, the fluctuations are more localized in the real space at the stable IR fixed point. Finally we discuss the imprints of such quasiparticleless metallic states at finite temperature and frequency, i.e. within the critical cone shown in Fig. 2.

The correlation lengths (along  $\hat{x}$ ) for the topological (between the DSM or nodal-loop semimetal and BI) and ordering (between the ASM and a broken symmetry phase) transitions are given by  $\xi_\Delta \sim |\Delta|^{-\nu_\Delta z_{\mathbf{k}}}$  and  $\xi_M \sim |M^2|^{-\nu_M z_{\mathbf{k}}}$ , respectively. On approaching the multicritical point both  $\xi_\Delta$  and  $\xi_M$  diverge faster than the mean-field expectation  $\xi_X \sim |X|^{-1}$ , where  $X \in \{\Delta, M\}$ . Since the dynamical exponent with respect to  $x$  is 1, the temperature scale ( $T_*$ ) associated with the transitions, tuned by  $X = \Delta$  and  $M$ , is given by  $T_* \sim \xi_X^{-1}$ . At the QCP the spectral density function measured at the erstwhile band-touching point scales as  $\mathcal{A}(\omega) \sim \omega^{-1+2\eta_\psi}$ . The dynamical structure factors for the order parameter fluctuations goes as  $\mathcal{S}(\omega) \sim \omega^{-1+2\eta_\phi}$ . Within the critical cone the specific heat and compressibility scale as  $C \sim T^{1+d_Q/z_{\mathbf{k}}}$  and  $\kappa \sim T^{d_Q/z_{\mathbf{k}}}$ , respectively. And specifically in two dimensions the optical conductivity of the non-Fermi liquid along  $\hat{x}$  and  $\hat{y}$  are respectively given by  $\sigma_{xx} \sim \omega^{-1/2+2\eta_\psi}$  and  $\sigma_{yy} \sim \omega^{1/2+2\eta_\psi}$ .

*Discussion:* We introduced a new classification scheme to tie together a large set of nodal-point semimetals, by tuning the number of linearly ( $d_L$ ) and quadratically ( $d_Q$ ) dispersing directions, see Fig. 1. Such a unifying scheme allows us to address emergent quantum critical phenomena in strongly interacting semimetallic systems, falling outside the jurisdiction of well studied DSMs, by employing suitable perturbative  $\epsilon$  expansions, when in particular these systems reside at the verge of a spontaneous symmetry breaking. As a demonstrative example, we here address this phenomenon in 2d-ASM ( $d_L = d_Q = 1$ ) and 3d-ASM<sub>1</sub> ( $d_L = 1, d_Q = 2$ ) in terms of an  $\epsilon$  expansion, where  $\epsilon = 2 - d_Q$  [see Table 1]. Specifically, our predicted quantum critical behavior for a two-dimensional ASM can be relevant for uniaxially strained optical honeycomb lattice [7–9] and artificial graphene [36], interface of

TiO<sub>2</sub>/VO<sub>2</sub> [12, 13], black phosphorus [11] and  $\alpha$ -(BEDT-TTF)<sub>2</sub>I<sub>3</sub> [10], and can also be tested in quantum Monte Carlo simulations of extended Hubbard model [37–40].

We close the discussion by presenting a comparison between quantum criticalities of a Fermi surface and an ASM. In both systems the Landau damping is responsible for the emergent non-Fermi liquid behavior. In the former system, however, the damping scale competes with that of a spontaneous symmetry breaking due to a finite DoS, which generally results in superconductivity at low temperatures [41]. By contrast, in an ASM the non-Fermi liquid behavior is expected to survive down to arbitrary low energies (a ‘naked’ QCP) due to the vanishing DoS. Moreover, the non-interacting Hamiltonian of a  $d_Q$  dimensional ASM is similar to those in patch-theories of Fermi surface QCPs [42], with the difference arising from the pole structure of the respective fermion propagators. Nonetheless, similar quantum dynamical structures suggest intriguing parallels between the low energy dynamics at these two classes of criticalities, which we will explore in future works.

*Acknowledgments:* S.S. was supported in parts by the National Science Foundation No. DMR-1442366, and the start-up funds of Pallab Goswami from Northwestern University. S.S. thanks Sung-Sik Lee and Sedigh Ghamari for helpful comments.

- 
- [1] M. Z Hassan, and C. L. Kane, *Rev. Mod. Phys.* **82**, 3045 (2010).
- [2] X. L. Qi, and S.-C. Zhang, *Rev. Mod. Phys.* **83**, 1057 (2011).
- [3] N. P. Armitage, E. J. Mele, A. Vishwanath, *Rev. Mod. Phys.* **90**, 015001 (2018).
- [4] G. E. Volovik, *The Universe in a Helium Droplet* (Oxford University Press, New York, 2003).
- [5] S.-Q. Shen, *Topological Insulators: Dirac Equation in Condensed Matters* (Springer, 2013).
- [6] B. Bradlyn, J. Cano, Z. Wang, M. G. Vergniory, C. Felser, R. J. Cava, B. A. Bernevig, *Science* **353**, aaf5037 (2016).
- [7] L. Tarruell, D. Greif, T. Uehlinger, G. Jotzu, and T. Esslinger, *Nature* **483**, 302 (2012).
- [8] T. Uehlinger, G. Jotzu, M. Messer, D. Greif, W. Hofstetter, U. Bissbort, and T. Esslinger, *Phys. Rev. Lett.* **111**, 185307 (2013).
- [9] M. Tarnowski, M. Nuske, N. Fläschner, B. Rem, D. Vogel, L. Freystatzky, K. Sengstock, L. Mathey, and C. Weitenberg, *Phys. Rev. Lett.* **118**, 240403 (2017).
- [10] A. Kobayashi, S. Katayama, Y. Suzumura, and H. Fukuyama, *J. Phys. Soc. Jpn.* **76**, 034711 (2007).
- [11] J. Kim, S. S. Baik, S. H. Ryu, Y. Sohn, S. Park, B.-G. Park, J. Denlinger, Y. Yi, H. J. Choi, and K. S. Kim, *Science* **349**, 723 (2015).
- [12] V. Pardo and W. E. Pickett, *Phys. Rev. Lett.* **102**, 166803 (2009).
- [13] S. Banerjee, R. R. P. Singh, V. Pardo, and W. E. Pickett, *Phys. Rev. Lett.* **103**, 016402 (2009).
- [14] B. Roy and M. S. Foster, *Phys. Rev. X* **8**, 011049 (2018).
- [15] H. Isobe, B.-J. Yang, A. Chubukov, J. Schmalian, and N. Nagaosa, *Phys. Rev. Lett.* **116**, 076803 (2016).
- [16] G. Y. Cho and E.-G. Moon, *Sci. Rep.* **6**, 19198 (2016).
- [17] C. Bollini and J. Giambiagi, *Phys. Lett. B* **40**, 566 (1972).
- [18] G. t’ Hooft and M. Veltman, *Nucl. Phys. B* **44**, 189 (1972).
- [19] K. G. Wilson and M. E. Fisher, *Phys. Rev. Lett.* **28**, 240 (1972).
- [20] J. Zinn-Justin, *Quantum Field Theory and Critical Phenomena* (Oxford University Press, Oxford, UK, 2002).
- [21] See, however, L. Janssen and I. F. Herbut, *Phys. Rev. B* **92**, 045117 (2015), for example.
- [22] Here  $f_1(x) = \left(\frac{\pi^2 \epsilon^{1/2}}{8}\right)^{1/x}$  and  $f_3(x) = \left(\frac{\pi^2 \epsilon^{5/2}}{8}\right)^{-1/x}$ .
- [23] The interacting fixed point ( $g_*^2$ ) exists for any  $N_b$  and  $N_f$  when  $0 < \epsilon \leq 1$  [see Eq. (6)], although the anomalous dimensions tend to vanish close to  $\epsilon = 1$ . This feature is, however, only an artifact of leading order  $\epsilon$  and  $1/N_f$  expansions. The precise values of these quantities can only be estimated after accounting for higher order corrections and subsequently performing a series resummation.
- [24] This is equivalent to setting an ultraviolet scale that is lower than the crossover scale below which quantum fluctuations dominate over the high energy term  $c^2|\mathbf{q}|^2$ .
- [25] D. Dalidovich and S.-S. Lee, *Phys. Rev. B* **88**, 245106 (2013).
- [26] C. Fang, Y. Chen, H.-Y. Kee, and L. Fu, *Phys. Rev. B* **92**, 081201 (2012).
- [27] B. Roy, *Phys. Rev. B* **96**, 041113 (2017).
- [28] S. Sur and R. Nandkishore, *New J. Phys.* **18**, 115006 (2016).
- [29] G. Xu, H. Weng, Z. Wang, X. Dai, and Z. Fang, *Phys. Rev. Lett.* **107**, 186806 (2011).
- [30] C. Fang, M. J. Gilbert, X. Dai, and B. A. Bernevig, *Phys. Rev. Lett.* **108**, 266802 (2012).
- [31] P. Dietl, F. Piéchon, and G. Montambaux, *Phys. Rev. Lett.* **100**, 236405 (2008).
- [32] J.-R. Wang, G.-Z. Liu, and C.-J. Zhang, *Phys. Rev. B* **95**, 075129 (2017).
- [33] Y.-M. Dong, D.-X. Zheng, and J. Wang, arXiv:1806.03410
- [34] See Supplementary Materials for additional details.
- [35] S. Sur and S.-S. Lee, *Phys. Rev. B* **94**, 195135 (2016).
- [36] K. K. Gomes, W. Mar, W. Ko, F. Guinea and H. C. Manoharan, *Nature (London)* **483**, 306 (2012).
- [37] F. F. Assaad and I. F. Herbut, *Phys. Rev. X* **3**, 031010 (2013).
- [38] Y. Otsuka, S. Yunoki, and S. Sorella, *Phys. Rev. X* **6**, 011029 (2016).
- [39] S. Pujari, T. C. Lang, G. Murthy, R. K. Kaul, *Phys. Rev. Lett.* **117**, 086404 (2016).
- [40] T. C. Lang and A. M. Läuchli, arXiv:1808.01230
- [41] M. A. Metlitski, D. F. Mross, S. Sachdev, and T. Senthil, *Phys. Rev. B* **91**, 115111 (2015).
- [42] I. Mandal and S.-S. Lee, *Phys. Rev. B* **92**, 035141 (2015).